

Pressure sensing recognition of FBG array based on random forest algorithm*

WANG Yan**, ZHU Wei, GE Ziyang, WANG Junliang, XU Haoyu, and JIANG Chao

School of Electrical and Information Engineering, Anhui University of Technology, Maanshan 243000, China

(Received 14 November 2022; Revised 15 January 2023)

©Tianjin University of Technology 2023

In order to improve the precision of static load pressure recognition and identify the position of the applied force accurately, a fiber Bragg grating (FBG) flexible sensor array is proposed in this work. Numerical analysis for the package thickness (4 mm) and package position (2 mm from the bottom) of the FBG flexible sensor is performed using COMSOL, and optimal package thickness (4 mm) and package position (2 mm from the bottom) are selected in the analysis. By using 12-FBGs layout method and random forest algorithm, the position and load prediction model is established. The results show that the average error of the distance between the prediction points of coordinates X - Y and static load F and the real sample points is 0.092. Finally, to verify the proposed models, the pressure sensing experiments of the flexible FBG array are carried out on this basis. The weights of 100 g to 1 000 g are applied to different regions of the flexible sensor array one by one in accordance with a certain trajectory. The variation of each FBG wavelength was taken as the input of the stochastic forest prediction model, and the coordinate position and the static load size F were taken as the output to establish the prediction model. The minimum distance error between the actual point and the predicted point was calculated by experiment as 0.034 91. The maximum is 0.248 1, and the mean error is 0.151 5. It is concluded that the random forest prediction model has a good prediction effect on the pressure sensing of the flexible FBG sensing array.

Document code: A **Article ID:** 1673-1905(2023)05-0262-7

DOI <https://doi.org/10.1007/s11801-023-2192-0>

In the research on structural monitoring, behavior monitoring, intelligent prosthetics, human-computer interaction and other aspects, tactile/pressure sensors with high sensitivity and accuracy have attracted increasing attention^[1-3]. At present, the common tactile/pressure detection methods include resistive^[4], piezoelectric^[5,6] and capacitive^[7], etc. However, the detection principle is basically based on the conversion of electrical signals, which will inevitably be affected by electromagnetic interference.

In recent years, optical fiber sensors have been widely used in intelligent structure monitoring and pressure sensing because of their unique characteristics of anti-electromagnetic interference, small size, easy embedding and high sensitivity. ZHANG et al^[8] used femtosecond laser technology to form microcavities by etching on single-mode fibers and coreless fibers, which are fabricated by fusion splicing into micro and nano low-temperature fiber pressure sensors, which measured a sensitivity of 110.33 mm/MPa at -196 °C. SOSAMMA et al^[9] made a tactile sensor with fiber Bragg grating (FBG) embedded in silica gel for imaging. The sensor is in contact with the detection surface, and detects the force perpendicular to the elastic polymer surface through the grating wavelength change, and is highly sensitive to the detection of 0.5 mm width notch. In

terms of localization, XIONG et al^[10] combined the correlation bits of the impact response signal and used a three-circle take intersection algorithm to localize the coordinates of the impact point in the impact region to which the plate structure is subjected by a 6-FBGs layout method with an average error of 3.5 cm. The fractal dimension is used as the impact characteristic quantity in this method, and the linearity between it and the impact location is poor. CHEN et al^[11] proposed an impact load location method based on the fractal box dimension of partial least square regression (PLSR). This study improved the robustness of the model, but it could not be located when the fractal dimension in y direction is low. WANG et al^[12] proposed 3-FBGs laying methods for impact positioning monitoring of aluminum plate, and obtained the group velocity dispersion curve of Lamb waves by using time-frequency wavelet analysis. According to the triangulation algorithm, the collision coordinates were determined, and the average positioning accuracy error was 30.89 mm. However, the sensitivity of FBG to Lamb wave detection in different directions is different, and coordinate error exists when three FBGs are set on aluminum plate during the experiment.

In this work, a flexible pressure sensing array system is proposed. By using 12-FBGs arrangement, the

* This work has been supported by the Provincial Science and Technology Major Project of Anhui Province (No.201903a05020029).

** E-mail: wangyan@ahut.edu.cn

detection part is evenly divided into 16 square areas with a width of 50 mm. This arrangement method not only reduces the coordinate error of FBGs, but also improves the accuracy of positioning recognition. The polydimethylsiloxane (PDMS) encapsulation method is used to improve the sensitivity of FBG detection, and combined with the random forest algorithm processing method, the FBG perception prediction of pressure sensing is realized.

The fiber core of the fiber grating sensor is mainly made of quartz material, and the period and refractive index of the grating will change when the external air pressure, temperature, humidity, strain, etc change slightly, resulting in a shift of the central wavelength^[13]. When the broadband light source propagates in the fiber, a part of the light will be reflected back by the grating when the light propagates to the grating area, and the reflected wavelength λ_B satisfies

$$\lambda_B = 2n_{\text{eff}}\Lambda. \quad (1)$$

When the optical fiber grating sensor is subjected to external forces and strain from the elastomer, the refractive index inside the optical fiber will change and an elastomeric effect will occur, at which time the change in wavelength of the grating reflected wave center $\Delta\lambda_B$ is

$$\Delta\lambda_B = 2n_{\text{eff}}\Lambda \left\{ 1 - \frac{n_{\text{eff}}^2}{2} [P_{12} - \nu(P_{11} + P_{12})] \right\} \cdot \varepsilon + 2n_{\text{eff}}\Lambda(\alpha + \xi) \cdot \Delta T, \quad (2)$$

where P_{11} and P_{12} are the effective elastic-optical coefficients, ε and ΔT denote the amount of change in strain and temperature over a period of time, respectively, ξ is the thermo-optical coefficient of the quartz fiber, usually $\xi=7 \times 10^{-6} \text{ nm}/^\circ\text{C}$, $\alpha=5.5 \times 10^{-7} \text{ nm}/^\circ\text{C}$, and ν denotes the Poisson's ratio of the fiber. The amount of change in the external environment is detected by demodulation based on the amount of change in reflected wavelength.

Since the PDMS material has the advantages of low elastic modulus, softness, corrosion resistance, and good deformation resistance, PDMS is selected as the packaging substrate in this paper, and the sensor is embedded to form an FBG flexible sensor^[14-16]. First draw a PDMS matrix encapsulation material with a length of 200 mm, a width of 200 mm and a height of 4 mm in the geometry of the component, and then set up a 30-mm-long optical fiber with a core and cladding outer diameter of 0.125 mm at half the height of the substrate, the position of the FBG is at the center of the fiber core. Since the grating is formed after fiber laser writing, and the material properties and mechanical properties of the fiber core, cladding and coating are very similar, and the overall properties do not change much, the grating can be treated as a fiber core^[17]. A cylinder with a radius of 10 mm and a height of 1 mm is set at the center of the substrate to simulate the forward static load

applied to the flexible FBG with material properties of Steel AISI 4340, and Tab.1 shows each material parameter.

After the material parameters are set, the magnitude of the load F is varied by setting the domain point probe at the center of the substrate and adding a parametric sweep with a range of [1 N, 10 N] in steps of 1 N. In this range, the relationship between the load and the stress value of the domain point probe can be obtained.

Tab.1 Material parameters

Material	Poisson's ratio	Young's modulus (GPa)	Density (kg/m ³)
Optical fiber	0.17	72	2 203
PDMS	0.48	1.2	1 084
Steel AISI 4340	0.28	205	7 850

Fig.1 shows the stress diagrams of the flexible FBG sensor under different loads, where (a) shows the stress diagrams of the flexible substrate and the optical fiber at $F=10 \text{ N}$. Fig.2(b), (c) and (d) show $F=1 \text{ N}$, $F=5 \text{ N}$ and $F=10 \text{ N}$, respectively. It can be seen that the deformation of the flexible substrate and the optical fiber gradually increases with the increase of the load F .

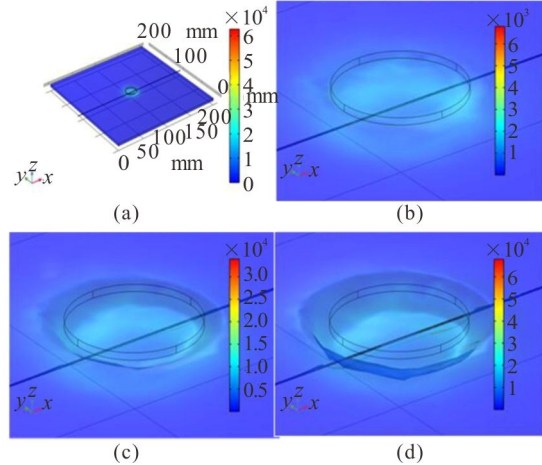


Fig.1 Strain diagram of flexible sensor

Firstly, the influence of the thickness of the package substrate on the FBG flexible sensor is explored. In the simulation, the substrate thickness is set to 3 mm, 4 mm, 5 mm, and 6 mm, and a load in the range of [1 N, 10 N] is applied to the substrate. The load and stress data for different package thicknesses were fitted using polynomials in the MATLAB linear fitting toolbox. Fig.2 shows the linear fitting of different package thicknesses. It can be obtained that the correlation coefficient R^2 is 1 when the package thickness is 3 mm, 4 mm and 5 mm, and the correlation coefficient R^2 is 0.990 4 when the package thickness is 6 mm. Among several different package thicknesses, the root mean square error (RMSE) is the smallest when the package thickness is 4 mm

(0.044 96), and the maximum *RMSE* (1 124) is achieved when the package thickness is 6 mm. Considering the linear relationship between the flexibility of the flexible packaging matrix and the load, the optimal packaging thickness of optical fiber is PDMS of 4 mm substrate. After confirming the encapsulation thickness, change the encapsulation position of the optical fiber to study the encapsulation at positions respectively 1 mm, 2 mm and 3 mm from the bottom surface. MATLAB is also used to linearly fit three different packaging positions, as shown in Fig.3. It can be obtained that the optical fiber packaging position is 2 mm from the substrate, the *RMSE* is the smallest (0.449 6), and the correlation coefficient R^2 is 1.

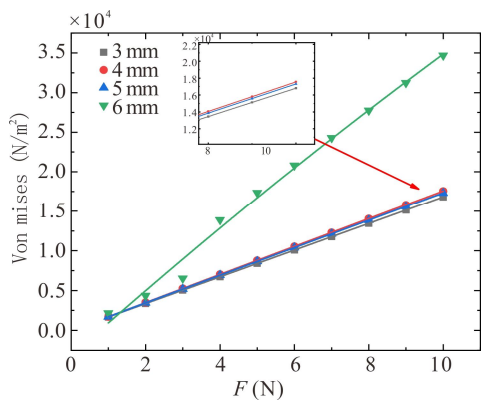


Fig.2 Stress curve of the flexible substrate with different package thicknesses

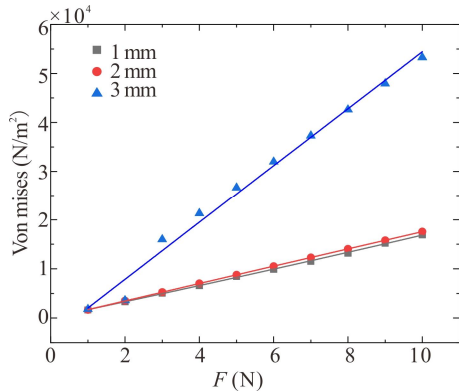


Fig.3 Stress curve of the flexible substrate with different packaging positions

Classification and regression tree (CART) is a learning algorithm that takes as output the probability distribution of the state of a random variable Y given a random variable $X^{[14]}$. The generation of the CART tree is a recursive process from top to bottom in the binary tree. Assuming that X and Y are input variables and output variables, respectively, x_i is the input value, and y_i is the mark value, then the specified training data set D is

$$D = \{(x_1, y_1), (x_2, y_2), \dots, (x_N, y_N)\}. \quad (3)$$

Each regression tree corresponds to a divided space, and there are corresponding input and output units in this

space. It is assumed that the input space has been divided into M units, which are R_1, R_2, \dots, R_m , and the output is fixed in each unit R_m , c_m , $I(x)$ is the indicator function, then the regression tree model and output value are shown as

$$f(x) = \sum_{m=1}^M c_m I(x \in R_m). \quad (4)$$

After the input space division of each regression tree is determined, the squared error is usually used as the estimated value of the regression tree and the deviation of the label, and then the square error minimum criterion method is used to obtain the best output value of each unit.

$$\sum_{x_i \in R_m} (y_i - f(x_i))^2. \quad (5)$$

It can be seen from the above formula that the optimal value c_m^* on R_m is the average value of the labels y_i corresponding to all input instances x_i on R_m , that is

$$c_m^* = \text{ave}(y_i | x_i \in R_m). \quad (6)$$

Select the j variable $x(j)$ and its value s as the segmentation variable and segmentation point, and define two regions, shown as

$$R_1(j, s) = \{x | x(j) \leq s\}, R_2(j, s) = \{x | x(j) > s\}. \quad (7)$$

Test each variable to find the best split variable j , let it form a number pair (j, s) and then divide the input space into two parts in order. Each region is segmented repeatedly until the termination condition is reached, and then a least squares regression tree is generated.

As shown in Fig.4, the sample set is used as the training set, and a training subset is extracted from the training set for a certain feature study. Multiple training subsets are combined to form a random forest model after processing through a CART regression tree. After the prediction set is substituted into the random forest model and processed, the model produces the output of the prediction set.

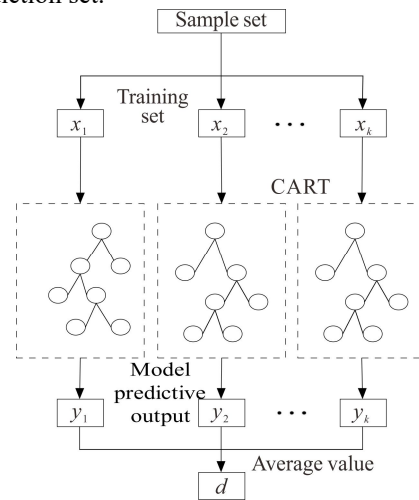


Fig.4 Random forest training model

In the random forest algorithm, *RMSE* and coefficient of determination (R^2) are usually used to judge the

prediction effect of the model. The smaller the *RMSE* value is, the closer the real value is to the predicted value, and the better the prediction effect is. The smaller the *RMSE* value, the closer the true value is to the predicted value, and the better the prediction is. The decision coefficient R^2 indicates the closeness of the correlation between the predicted and true values, and the correlation is better when R^2 is closer to 1^[18].

$$R^2 = 1 - \frac{\sum_{i=1}^n (y_i - \hat{y}_i)^2}{\sum_{i=1}^n (y_i - \bar{y}_i)^2}, \tag{8}$$

$$RMSE = \sqrt{\frac{\sum_{i=1}^n (y_i - \hat{y}_i)^2}{n-1}}. \tag{9}$$

The flexible PDMS substrate with length, width, and height of 200 mm, 200 mm, and 4 mm, respectively, is divided in units of 50 mm to obtain a total of 16 independent regions. As shown in Fig.5, 12 domain point probes are added as inspection locations, and Steel AISI 4340 is made to apply load F (1 N, 10 N) to each region in sequence by parametric scanning with a step size of 1 N. The motion trajectory is shown in Fig.6.

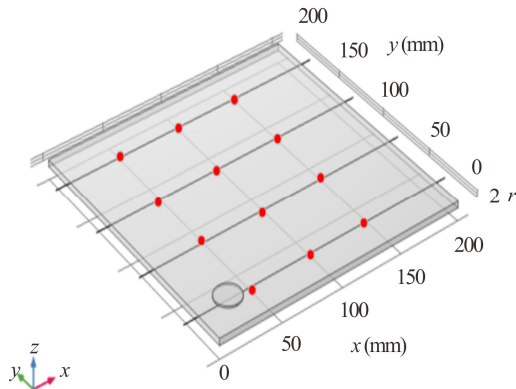


Fig.5 Domain point probe distribution

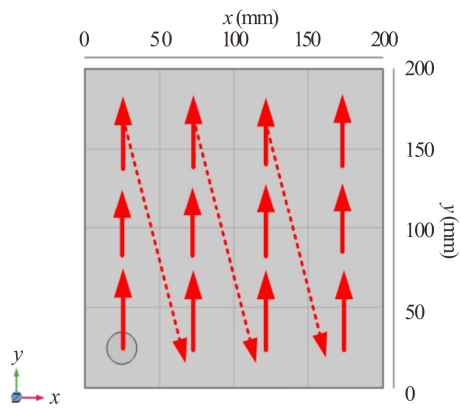


Fig.6 Load motion trajectory diagram

First, the stress values detected by the 12 domain point probes are used as the input values of the model, and the X -axis coordinates, Y -axis coordinates, and F are used as the output values. Then 128 of the 160 data sets are used

as training values and the remaining 32 data sets are used as predicted values, and the measured data are processed by the random forest algorithm to obtain the 12-FBGs evaluation indexes in the simulation model as shown in the following Tab.2.

Tab.2 Simulation model evaluation index

		X	Y	F
12-FBGs	<i>RMSE</i>	0.061 331	0.038 505	0.079 325
	R^2	0.996 2	0.998 7	0.999 1

20% of the 160 data is randomly selected as the test set sample, and the error comparison between the prediction point and the theoretical point is made on the test sample, as shown in Fig.7. The average error of 12-FBGs layout is 0.092 0 by calculation.

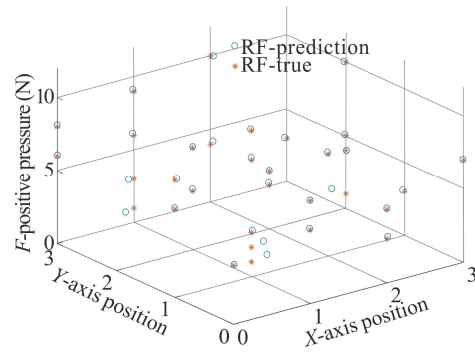


Fig.7 Test set error comparison

Four customized FBG fiber grating strings with three FBGs of different center wavelengths on each fiber string, and the parameters of the center wavelength of each string are shown in Tab.3. In this experiment, the flexible FBG sensor is protected by using silica gel solution of HC-820.

Tab.3 FBG fiber string peak parameters

Sample	Central wavelength (nm)		
FBG-1	1 529.922 3	1 535.141 3	1 539.893 8
FBG-2	1 534.188 4	1 539.028 4	1 543.885 3
FBG-3	1 543.005 1	1 547.994 9	1 552.883 1
FBG-4	1 551.026 3	1 555.904 3	1 561.178 5

The experimental system is shown in Fig.8. The demodulation equipment of the experiment is MOI Si-155, the wavelength range is 1 460—1 620 nm, the demodulation accuracy is 1 pm, and the measurement frequency is 1 000 Hz. A load is applied at the location of the sensing array area using weights following a certain trajectory, and the flexible sensing array is deformed due to the influence of the load, resulting in a shift of the central wavelength of the FBG in the sensing array. The wavelength change of the FBG within a certain time is used as the characteristic data, and the magnitude and

position of the load is predicted according to the change of the characteristic data.

Random forest is a kind of machine learning method. The advantages of machine learning are that the training time is short, and a large number of data sets are not required as training sets. The variation of central wavelength of each FBG in the collected data shows that the variation of central wavelength of FBG is different when static load is added in different position regions. Therefore, when building the prediction model, the change of central wavelength of 12-FBGs is taken as the input data, and the static load value and position coordinate are taken as the output data, respectively.

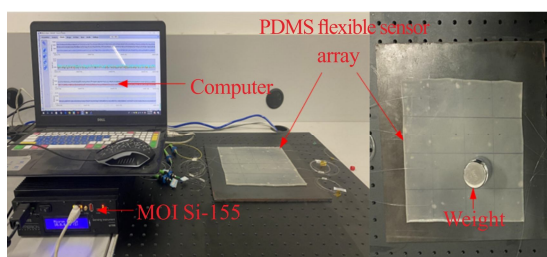


Fig.8 Flexible FBG sensing array experimental system

During the experiment, the movement trajectory of the weight is shown in the figure. The weight mass ranges from 100 g to 1 000 g. Firstly, the 100 g weight is applied to 16 regions successively according to the moving track. Each time the weight is applied, the wavelength variation data of 12-FBGs for 5 s are recorded. The weights are replaced with 100 g steps and the above steps are repeated. A total of 160 sets of sample data are recorded. Finally, the collected sample data is processed to calculate the difference between the central wavelength of each FBG and the initial central wavelength under different positions and loads, and the corresponding position coordinates and static load size are saved. 128 groups of data are selected from 160 groups of data as the training set, 128 groups of data are processed by the algorithm, the change of each grating center wavelength is taken as the input value, the coordinate (x, y) and its load F is taken as the output value, and the input-output mapping relationship is established. The remaining 32 groups of data are substituted into the algorithm as predicted values for random forest prediction. The predicted results are shown in Tab.4.

Tab.4 Static load test evaluation parameters of the flexible FBG sensing system

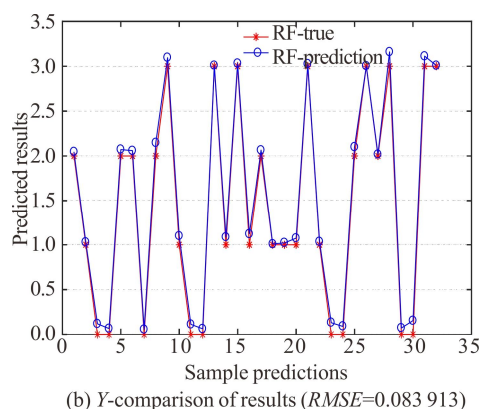
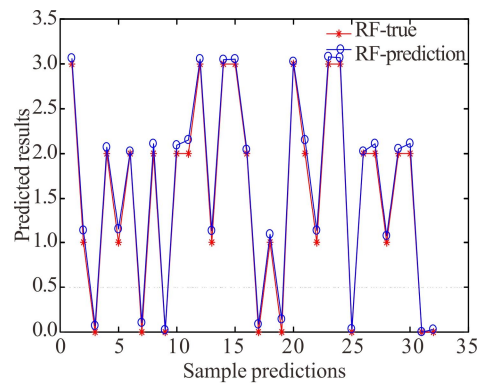
		X	Y	F
12-FBGs	RMSE	0.089 982	0.083 913	0.091 134
	R^2	0.992 2	0.992 0	0.998 9

By comparing the distance between the prediction of three characteristic quantities X , Y and F and the real

value, it can be seen from Fig.9 that the distance error predicted by the random forest regression model in the X -coordinate (0—3) region is less than 0.15 for 30 cases, and the minimum distance error is 0.006 6 and the maximum is 0.158 8. The distance error predicted by the random forest regression model of Y -coordinate (0—3) region is less than 0.15 in 30 cases, and the minimum distance error is 0.003 2 and the maximum distance error is 0.158 9. The distance error predicted by random forest regression model of load size F (1 N, 1 N, 10 N) is less than 0.15 in 29 cases, and the minimum distance error is 0.013 and the maximum distance error is 0.156 2.

As shown in Fig.10, the minimum distance error between the real value and the theoretical value of 32 groups of sample points is 0.034 91, and the average error is 0.151 5. There are 31 sample points with distance error less than 0.24.

In this work, a pressure sensing system of FBG array combined with random forest algorithm is proposed. Random forest is a machine learning method which the training time is short, and a large number of data sets are not required as training sets. Since random forest cannot predict beyond the range of training set data, the prediction range of the algorithm can be effectively determined by establishing a model. In the training process, random forest can detect the influence relationship between features. Therefore, this paper chooses random forest as the processing algorithm of the FBG array pressure sensing system.



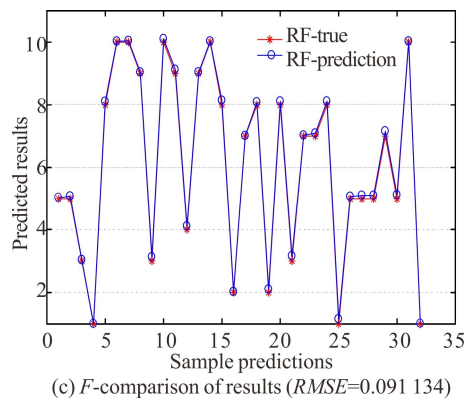


Fig.9 Static load prediction diagram of the flexible FBG array

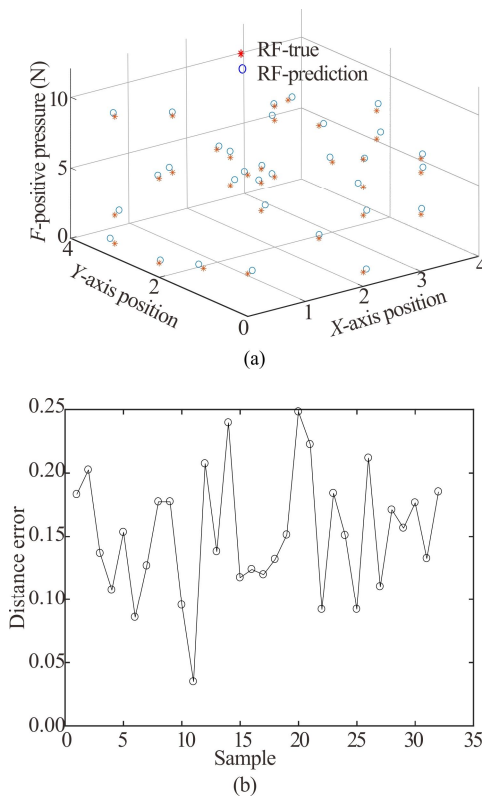


Fig.10 Pressure sensing prediction errors of the flexible FBG array

The fiber grating flexible PDMS sensor is built using COMSOL simulation software, and the effects of package thickness and package location on the stress transfer of the sensor are discussed. Meanwhile the corresponding COMSOL simulation model is established, and the physical quantity change of FBG position in the actual experiment is calculated by adding domain point probes, and the experimental system is built according to the simulation as well as the random forest algorithm identification results, and the prediction model with the central wavelength change amount as the input signal and the position and the positive load magnitude as the

output signal is established. It is concluded that the $RMSE$ is less than 0.1 and R^2 is greater than 0.99. The average error between the predicted and actual values is 0.151 5, and the random forest prediction model has a good prediction effect on the position and static load value of this flexible FBG sensing array. The room temperature was kept constant during the experiment to avoid the temperature cross-sensitivity of the FBG. The effect of temperature variation on the prediction accuracy of this model will be investigated in depth during the subsequent study.

Statements and Declarations

The authors declare that there are no conflicts of interest related to this article.

References

- [1] ZHAO Y, WANG T, ZHAO Z. Track-etch membranes as tools for template synthesis of highly sensitive pressure sensors[J]. *ACS applied materials & interfaces*, 2022, (1): 14.
- [2] ZHU Y Z, HARTEL M C, YU N, et al. Epidermis-inspired wearable piezoresistive pressure sensors using reduced graphene oxide self-wrapped copper nanowire networks[J]. *Small methods*, 2021, 6(1): 2100900.
- [3] YU C, DAN W C, SHA B, et al. Highly stretchable triboelectric tactile sensor for electronic skin[J]. *Nano energy*, 2019, 64: 103907.
- [4] WANG C, LI X, GAO E, et al. Wearable strain sensors: carbonized silk fabric for ultrastretchable, highly sensitive, and wearable strain sensors[J]. *Advanced materials*, 2016, 28(31): 6639-6639.
- [5] ZHANG Y, YE J, LIN Z, et al. A piezoresistive tactile sensor for a large area employing neural network[J]. *Sensors*, 2019, 19(1): 27-43.
- [6] FENG Z, ZHAO C, et al. Flexible piezoelectric-induced pressure sensors for static measurements based on nanowires/graphene heterostructures[J]. *ACS nano*, 2017, 11(5): 4507-4513.
- [7] YXA B, YSA C, LAN T A, et al. A flexible, ultra-highly sensitive and stable capacitive pressure sensor with convex microarrays for motion and health monitoring-ScienceDirect[J]. *Nano energy*, 2020, 70: 104436.
- [8] ZHANG Y T, JIANG Y, CUI Y, et al. Research on the micro optical fiber Fabry-Perot ultra-low temperature pressure sensor[J]. *Acta photonica sinica*, 2022, 51(05): 229-235. (in Chinese)
- [9] SOSAMMA S, ANISH K, CHANDAN K M. Fiber Bragg grating tactile sensor for imaging[J]. *Optik*, 2019, 198: 163062.
- [10] XIONG Z L, LIANG D K, LI T W, et al. Impact localization by using fiber Bragg grating sensors based on correlation dimension[J]. *Chinese journal of lasers*,

- 2016, 43(08): 203-211.
- [11] CHEN S B, PAN X W, LIU J F. Impact localization method based on the partial least squares regression fractal dimension[J]. Journal of vibration and shock, 2021, 40(02): 97-102.
- [12] WANG W, TAO C Y, ZHU Y Q, et al. Application of fiber Bragg grating sensor array in impact location monitoring[J]. Chinese journal of scientific instrument, 2022, 43(06): 76-82.
- [13] ZHANG X X, SONG Y M, MENG F Y, et al. Flexible composite skin embedded optical fiber shape sensing for variant aircraft[J]. Infrared and laser engineering, 2019, 48(06): 393-400.
- [14] WANG Y, QIN N, LIU J H, et al. Performance test of temperature and pressure flexible sensor based on optical fiber bragg grating[J]. Chinese journal of scientific instrument, 2019, 40(03): 93-98.
- [15] GE Z Y, WANG Y, QIN N, et al. Analysis of strain error of FBG flexible sensor with relative slip under vertical pressure[J]. Acta photonica sinica, 2020, 49(10): 43-51. (in Chinese)
- [16] JIN P, WANG Y, QIN N, et al. Relative slipping at the interfaces of the flexible fiber Bragg grating sensor[J]. Optoelectronics letters, 2021, 17(10): 604-610.
- [17] HE S J, LIU D T, PENG Y. Flight mode recognition method of the unmanned aerial vehicle based on telemetric data[J]. Chinese journal of scientific instrument, 2016, 37(09): 2004-2013.
- [18] FANG X R, WEN Z F, CHEN J L, et al. Remote sensing estimation of suspended sediment concentration based on random forest regression model[J]. Journal of remote sensing, 2019, 23(4): 756-772.